Extracting the dipole cross section from photo- and electroproduction total cross-section data

J. R. Forshaw,[1,*] G. Kerley,[2] and G. Shaw[2]

[1]*Theory Division, CERN, 1211 Geneva 23, Switzerland*
[2]*Department of Physics and Astronomy, University of Manchester, Manchester M13 9PL, England*

We report on a successful attempt to extract the cross section for the high-energy scattering of color dipoles of fixed transverse size off protons using electroproduction and photoproduction total cross-section data, subject to the constraint provided by the ratio of the overall photon dissociation cross section to the total cross section. [S0556-2821(99)04317-9]

I. INTRODUCTION

Photon-hadron interactions at high energies can be described in the rest frame of the hadron using a picture in which the incoming photon undergoes a fluctuation into virtual partonic or hadronic states, which subsequently interact strongly with the hadron. A number of singly dissociative diffractive processes, namely elastic Compton scattering, photon dissociation, exclusive vector meson production and deeply virtual Compton scattering, can be formulated in terms of a quantity, the *color dipole cross section*, which is universal for a given hadron target [1–4]. We report on a successful attempt to extract the cross section for scattering color dipoles of fixed transverse size off protons using both electroproduction and photoproduction γp total cross-section data, subject to the constraint provided by the ratio of the overall photon dissociation cross section to the total cross section.

We begin by briefly summarizing the color dipole model of diffraction; we then describe the assumed forms of the dipole cross section and the photon wave functions before discussing the data fits and the resulting values of the dipole cross section.

II. COLOR DIPOLES AND DIFFRACTION

A. γp total cross section

Our first task is to introduce the color dipole cross section and relate it to the γp total cross section. Here we follow closely the treatment of [5,6]. Of particular utility in the study of diffractive scattering is a decomposition of the strongly interacting fluctuations of the photon into a superposition of Fock states in the quark-gluon basis:

$$|\gamma\rangle = \sum |q\bar{q}\rangle + |q\bar{q}g\rangle + \text{higher Fock states.} \quad (1)$$

We define r as the transverse separation averaged over all orientations of the quark-antiquark pair and z as the fraction of the light-cone energy of the photon carried by one of the

---

*On leave of absence from the Department of Physics and Astronomy, University of Manchester, Manchester, M13 9PL, England.

pair (Fig. 1). Quark-antiquark states with definite values of z and r preserve these values during the diffractive process; or, to put it another way, they are eigenstates of the scattering matrix $\hat{T}$ when it is restricted to diffractive processes. This we shall call the diffraction operator. The quark-antiquark eigenstates are called *color dipoles*. Expanding the virtual photon in these states gives

$$|\gamma\rangle = \int dz\,d^2r\,\psi(z,r)|z,r\rangle + \text{higher Fock states,} \quad (2)$$

where $\psi(z,r)$ is the *light cone wave function* of the photon.

The diffractive process modulates the light cone wave function by the eigenvalue τ of the diffraction operator:

$$\hat{T}|z,r\rangle = i\tau(b,s;z,r)|z,r\rangle. \quad (3)$$

Here b is the *impact parameter* of the dipole with respect to the proton center, being a weighted sum of the individual impact parameters b_1, b_2 of its constituents [7]:

$$b = |\mathbf{b}|$$

$$\mathbf{b} = z\mathbf{b}_1 + (1-z)\mathbf{b}_2. \quad (4)$$

The factor i in Eq. (3) is inserted for convenience; it ensures that τ is predominantly real (since diffractive amplitudes are predominantly imaginary).

Consider the γ^*p total cross section in deep inelastic scattering. We first express the elastic scattering amplitude for $\gamma^*p \rightarrow \gamma^*p$ in terms of the Mandelstam variables $s = W^2$ and t, which can be done by a Fourier transform with respect to the momentum conjugate to b, namely the perpendicular part of the proton momentum transfer: $q' = p - p'$. So we arrive at

$$A^{el}(s,t) = \int d^2b\,e^{i\mathbf{q}'_\perp \cdot \mathbf{b}}\langle\gamma|\hat{T}|\gamma\rangle. \quad (5)$$

Use of the optical theorem leads to

$$\sigma_{T,L}^{\gamma^*p} = \int dz\,d^2r|\psi_\gamma^{T,L}(z,r)|^2 \int \frac{d^2b\,\tau(s,b;z,r)}{s}. \quad (6)$$

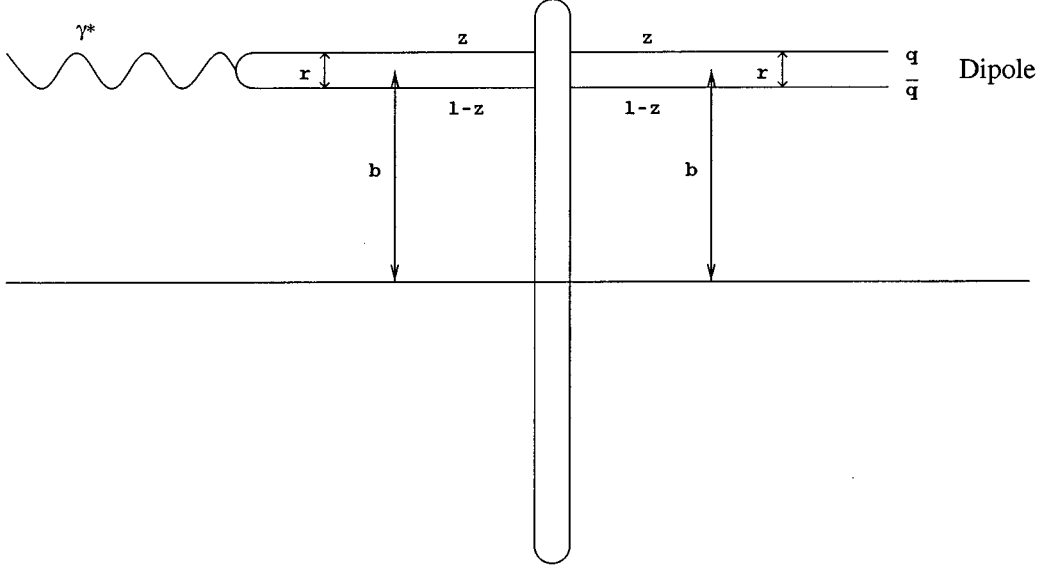The second integral expression defines the color dipole cross section:

FIG. 1. The diffractive process from a mixed position-momentum viewpoint. Transverse components are spatial; non-transverse components are light cone momenta.

$$\int \frac{d^2 b \, \tau(s,b;z,r)}{s} \equiv \sigma(s,r,z). \tag{7}$$

This is the total cross section for scattering dipoles of a specified configuration (z,r) off a proton.

B. Other processes

There are other interesting processes which involve the dipole cross section: vector meson production and photon dissociation. The formulation of the first is straightforward. The differential cross section is given by

$$\left. \frac{d\sigma_{T,L}^V}{dt} \right|_{t=0} = \frac{1}{16\pi} \left[\int dz d^2 r \, \psi_V^*(z,r) \psi_\gamma^{T,L}(z,r) \sigma(s,r,z) \right]^2. \tag{8}$$

For photon dissociation, we can express the final state as an incoherent sum of the diffractive eigenstates (dipole states) [6]:

$$\left. \frac{d\sigma_{T,L}^D}{dt} \right|_{t=0} = \frac{1}{16\pi s^2} \sum_k |\langle \gamma^{T,L} | \hat{T} | z,r \rangle|^2 \tag{9}$$

and hence

$$\left. \frac{d\sigma_{T,L}^D}{dt} \right|_{t=0} = \frac{1}{16\pi} \int dz d^2 r |\psi_\gamma^{T,L}(z,r)|^2 \sigma^2(s,r,z). \tag{10}$$

Note that only that subset of the diffractive dissociation final state which is composed exclusively of a quark-antiquark pair has been included in this expression.

The dipole cross section thus constitutes a link between three distinct physical processes. If the dipole cross section is known, then vector meson wave functions predicted from models can be inserted in Eq. (8) and the models tested by comparison of the result with experiment. Alternatively, the vector meson wave function itself can be extracted.

III. PARAMETRIC FORMS

In what follows, our aim is to extract the dipole cross-section from the total cross-section data for virtual photoabsorption by protons (structure function and real photoabsorption data), and to use the result to predict the contribution to the photon dissociation rate from dipole scattering. In order to do this, it is necessary to assume parametric forms for the dipole cross section which embody reasonable theoretical requirements, but are otherwise flexible. Here we describe the form used in our fits, together with our assumptions for the photon wave function.

A. Dipole cross section

The dipole cross section is in general a function of z, $s = W^2$ and r. However, a non-perturbative calculation reveals little z dependence [7] and we shall neglect it completely in what follows.

Following other authors [8,9] we assume the existence of two distinct terms which carry a Regge type s dependence: the hard term, which is assumed to dominate at small r but vanish in the limit of large r, and the soft term, with an s exponent close to zero, which is assumed to dominate at large r and saturate. Specifically, we assume

$$\sigma(s,r) = \sigma_{soft}(s,r) + \sigma_{hard}(s,r)$$

where the r dependences are given by

$$\sigma_{soft}(s,r) = a_0^S \left(1 - \frac{1}{1 + (a_1^S r + a_2^S r^2)^2} \right)(r^2 s)^{\lambda_S}$$
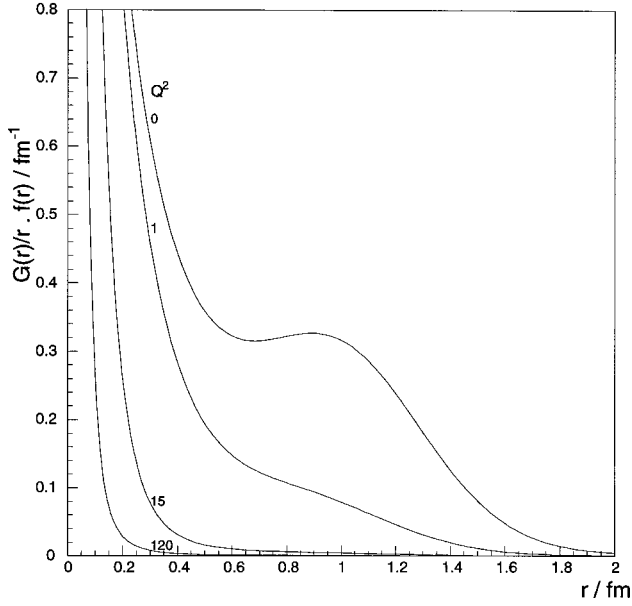
FIG. 2. The weight function $f(r)G(r)/r$ for different Q^2 (fit I). The peak at low Q^2 represents the modification to the photon wave function.

$$\sigma_{hard}(s,r) = (a_1^H r + a_2^H r^2 + a_3^H r^3)^2 \exp(-\nu_H^2 r)(r^2 s)^{\lambda_H}. \tag{11}$$

In these formulas the energy variable s has an associated r^2 factor, which yields an implicit Q^2 dependence and approximate scaling on integrating over the photon wave function. Apart from this, both terms possess a limiting r^2 dependence at small r in accordance with color transparency[1] arguments [11]. The squared polynomials in r provide a fine-tuning of the r dependence that is strictly non-negative.

B. Photon wave function

In the first instance, we used the tree level QED form of the photon light cone wave function:

$$|\psi_L(z,r)|^2 = \frac{6}{\pi^2} \alpha \sum_{q=1}^{n_f} e_q^2 Q^2 z^2 (1-z)^2 K_0^2(\epsilon r) \tag{12}$$

$$|\psi_T(z,r)|^2 = \frac{3}{2\pi^2} \alpha \sum_{q=1}^{n_f} e_q^2 \{ [z^2 + (1-z)^2] \epsilon^2 K_1^2(\epsilon r) + m_f^2 K_0^2(\epsilon r) \} \tag{13}$$

where

$$\epsilon^2 = z(1-z)Q^2 + m_f^2,$$

___

[1] Color transparency arguments usually assume a parametrization in x, which contains an implicit Q^2 dependence, rather than s. It is unnatural to have a Q^2 dependence in the dipole cross section itself [10] and we prefer to introduce it as the transform of an additional r dependence via the photon wave function.

TABLE I. Fit I, satisfying the ZEUS diffractive ratio for real photons.

Total χ^2 311 (0.88 per d.o.f.)			
λ_S	0.06 (fixed)	λ_H	0.387 ± 0.005
a_0^S	30.05 (fixed)		
a_1^S	0.12 ± 0.01	a_1^H	0.99 ± 0.07
a_2^S	-0.202 ± 0.005	a_2^H	0.7 ± 0.1
		a_3^H	-6.23 ± 0.08
		ν_H^2	4.36 ± 0.02
B	6.4 ± 0.1	c^2	0.205 ± 0.004
R	6.46 ± 0.03	m^2	0.08 (fixed)

Photoabsorption data ($Q^2 = 0$)		
Data set	Number of points	χ^2 per data point
Caldwell	18	1.5
H1	1	2.1
ZEUS	1	3.9

K_0 and K_1 are modified Bessel functions and the sum is over quark flavors. The quark masses can be neglected at large Q^2, but are important at low Q^2. Here we assume three light quark flavors with a generic value $m_f^2 = 0.08$ GeV^2. This corresponds roughly to a constituent quark mass and enables good fits to real as well as virtual photon data to be obtained. The use of a constituent as opposed to a current quark mass can be regarded as a partial reflection of confinement. Subsequently we found it necessary to incorporate other confinement effects in the wave function, as described below.

Finally, the absence of a z dependence in the dipole cross section allows us to explicitly integrate over it in Eq. (6) to give

$$\sigma_{tot}^{\gamma^* p} = \int dz \, d^2 r [|\psi_T(z,r)|^2 + |\psi_L(z,r)|^2] \sigma(s,r)$$

$$= \frac{6}{\pi^2} \alpha \sum_{q=1}^{n_f} e_q^2 \int d^2 r \frac{G(r)}{r^2} \sigma(s,r), \tag{14}$$

for $\sigma = \sigma_T + \sigma_L$, where

$$G(r) = \int_0^1 dz \, r^2 \left\{ \left[Q^2 z^2 (1-z)^2 + \frac{m_f^2}{4} \right] K_0^2(\epsilon r) + \frac{[z^2 + (1-z)^2] \epsilon^2 K_1^2(\epsilon r)}{4} \right\}. \tag{15}$$

IV. EXTRACTING THE DIPOLE CROSS SECTION

A. Data set

The F_2 data set consisted of HERA 1994 and 1995 data from the H1 [12,13] and ZEUS [14–17] experiments, together with the fixed target E665 values [18]. This was combined with the very precise intermediate energy photopro-

TABLE II. Fit II, satisfying the H1 diffractive ratio for real photons.

Total χ^2 310 (0.87 per d.o.f)			
λ_S	0.06 (fixed)	λ_H	0.380 ± 0.005
a_0^S	60.28 (fixed)		
a_1^S	0.032 ± 0.005	a_1^H	0.0 ± 0.07
a_2^S	-0.094 ± 0.002	a_2^H	7.9 ± 0.2
		a_3^H	-13.9 ± 0.1
		ν_H^2	4.91 ± 0.02
B	2.40 ± 0.05	c^2	0.152 ± 0.005
R	6.08 ± 0.05	m^2	0.08 (fixed)

Photoabsorption data ($Q^2=0$)		
Data set	Number of points	χ^2 per data point
Caldwell	18	1.5
H1	1	1.9
ZEUS	1	3.8

duction data [19] plus the two high energy points from H1 [20] and ZEUS [21] respectively. The following cuts were imposed:

(i) A cut in s ($s \geq 100$ GeV^2) to ensure the data was sufficiently high energy.

(ii) A cut in x ($0 \leq x \leq 0.01$) to ensure the data was diffractive.

(iii) A cut in Q^2 ($Q^2 \leq 60$ GeV^2).

Altogether there were 345 F_2 and 20 photoabsorption data points, compared to 10 adjustable parameters in our final fits, described below.

In fitting these data, the purely diffractive contribution described above was supplemented by a small non-diffractive component arising from the leading meson exchange trajectories. This was assumed to be given by the empirical Donnachie-Landshoff form [22]

$$F_2^R = 0.098 x^{0.4525} \left(\frac{Q^2}{Q^2+0.0111} \right)^{0.5475} \quad \text{(electroproduction)}$$

$$\sigma_{\gamma p}^R = 0.3318 s^{-0.4525} \text{ GeV}^{-2} \quad \text{(photoproduction)}. \qquad (16)$$

Its contribution was always less than 15% for photoproduction and typically 3% or less for electroproduction.

B. Fits

The inversion of integral equations of the type in Eq. (14) presents notorious problems of non-uniqueness and instability (sensitivity to small alterations in input data) of the resulting function [23,24]. Certain features of our fits, however, mitigate these effects. Our parametrization ensures that the dipole cross section is strictly positive, as is essential from its physical interpretation, and this already goes a long way to ensure that the output is robust towards data fluctuations. Further, we have imposed many additional constraints from physical considerations which limit the degree of arbitrariness in the final fit. Nevertheless, we were unable to
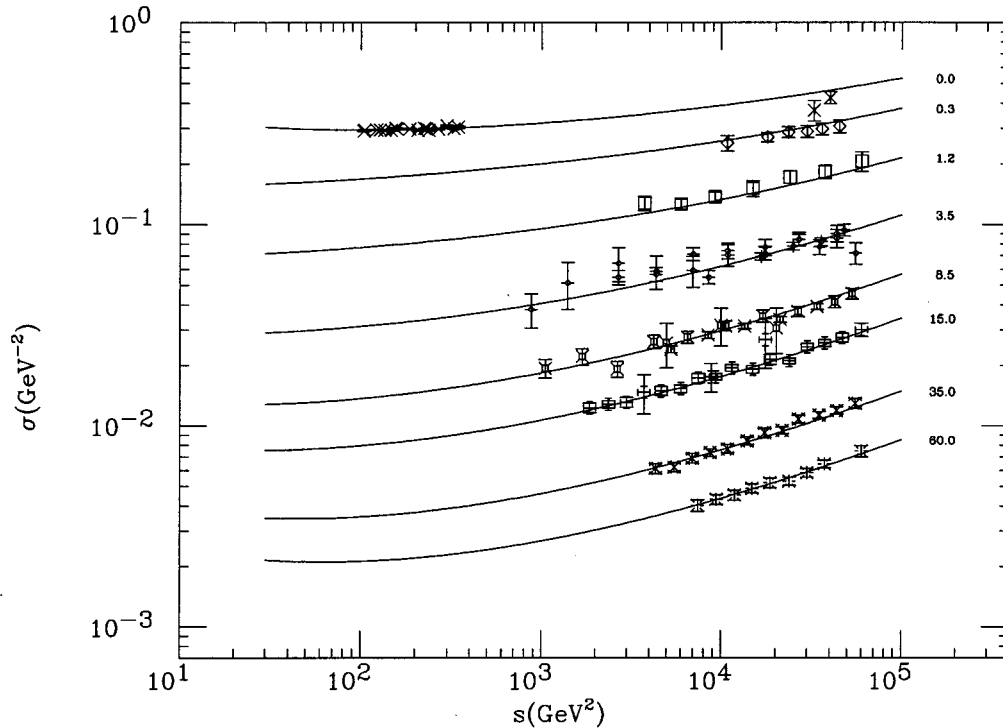

FIG. 3. Representative sample of fitted data points for the total cross section $\sigma_{\gamma p}^{tot}$ compared with curves calculated from the parametrized dipole cross section for different Q^2 values (fit I).
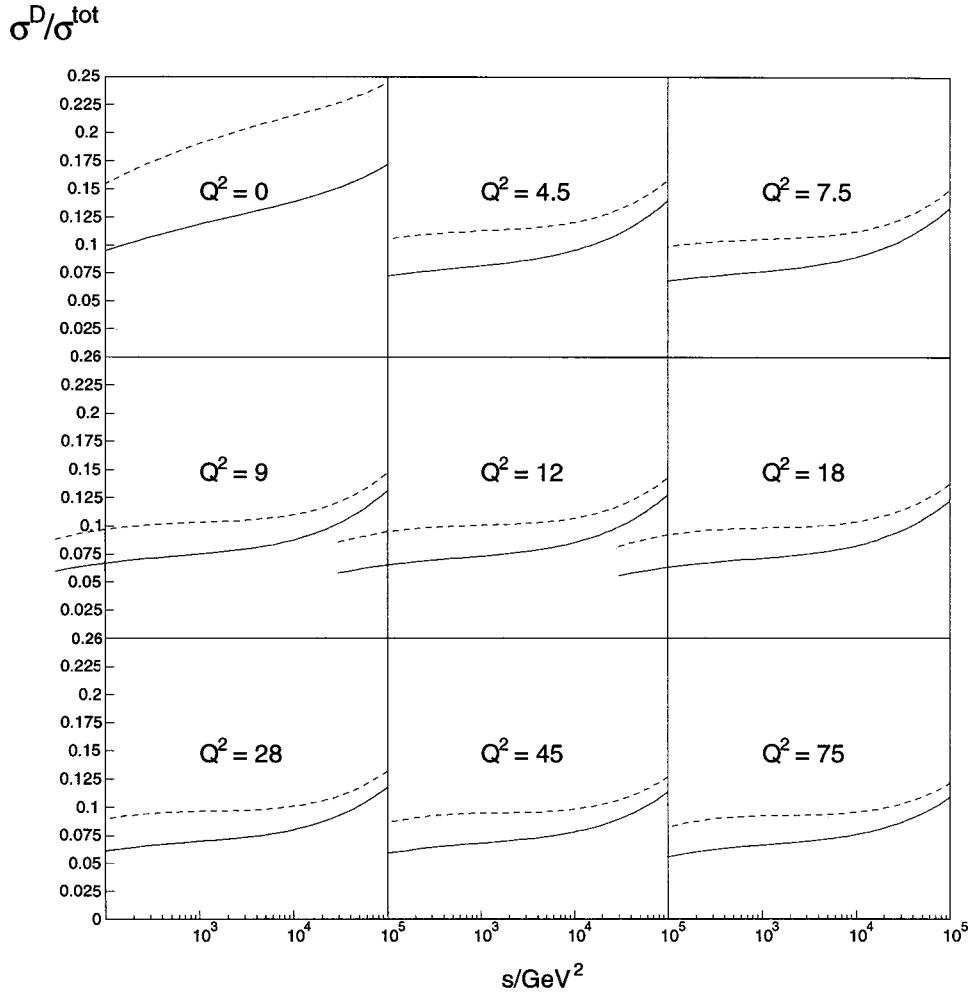
σ^D/σ^{tot}

FIG. 4. Ratio of the overall singly dissociative diffractive cross section to the total cross section for fit I (solid line) and fit II (dotted line).

achieve a positive definite error matrix for our fits so that the errors quoted below are approximate.

1. Fits with a QED wave function

Using the QED photon wave functions of Eq. (12) led to successful fits to the γp total cross-section data using the above and other similar parametrizations. However, although the χ^2 values typically ranged from 0.9 to 1.2 per degree of freedom (DOF), this was achieved at the price of unphysically large dipole cross sections for dipole sizes greater than or of order 1 fm. For example, these were found to be of order 100 mb at $\sqrt{s} = 100$ GeV, compared with a $\rho^0 N$ cross section of about 25 mb [25].

Such a large dipole cross section has the effect of predicting much too high a rate for diffractive processes, which are more sensitive to large dipoles since the dipole cross section is squared in Eq. (10). This rate can be calculated from our parametrization using Eq. (10) and integrating over t using the relation

$$\left.\frac{d\sigma^D}{dt}\right| = \left.\frac{d\sigma^D}{dt}\right|_{t=0} \exp(-b|t|), \qquad (17)$$

where for the slope parameter b we used the value 7.2 GeV^{-2} [26]. This leads to predicted diffractive cross sections which are typically over 45% of the total for real photons. In contrast, the experimental values are 22.2 $\pm 3.2\%$ ($s = 3.5 \times 10^4$ GeV^2) [27] according to the H1 Collaboration and $13.3 \pm 3.6\%$ ($s = 4 \times 10^4$ GeV^2) [28] according to the ZEUS Collaboration.

Thus, in spite of the apparent success of the fits, there are clearly serious shortcomings in the above approach. This is confirmed by both the flexibility of the functional forms chosen and the fact that we could not fit the data at all when we impose reasonable limits on the cross sections for large dipoles. The obvious suspect is the assumed form of the photon wave function at large transverse size, where confinement effects are surely significant.

2. Modifying the photon wave function

We adopt a pragmatic, *a posteriori* approach to this problem by modifying the photon wave function so that the soft contribution to the dipole cross section is brought into line with the above experimental constraints, while the hard contribution is unaltered.
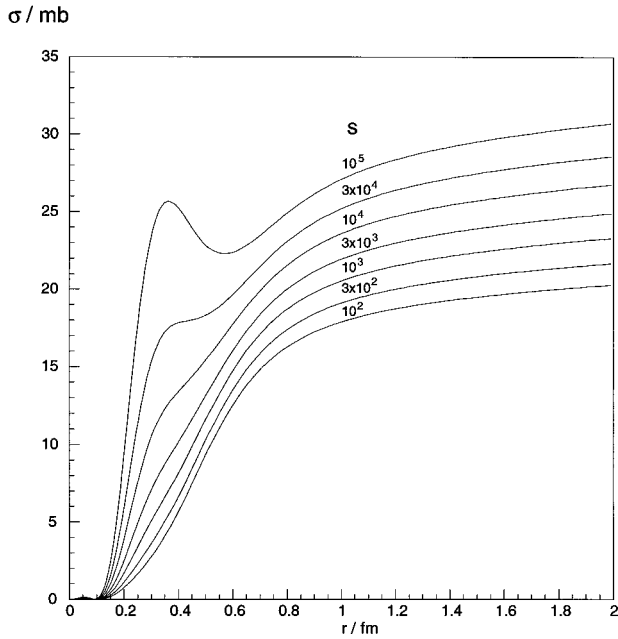
FIG. 5. The dipole cross section at different energies (fit I).

FIG. 7. The relative weighting of the contributions to the total photoabsorption cross sections from dipoles of different size (fit I).

As mentioned above, the high value for the diffractive to total cross-section ratio is indicative of inflated values of the dipole cross section at large r. If the photon wave function were larger at those large r values for which the integrand of Eq. (6) is still appreciable, then the value of the diffractive cross section would be smaller. Consequently, we multiply $G(r)$ by a shifted Gaussian:

$$f(r) = \frac{1 + B \exp[-c^2(r-R)^2]}{1 + B \exp(-c^2 R^2)}. \quad (18)$$
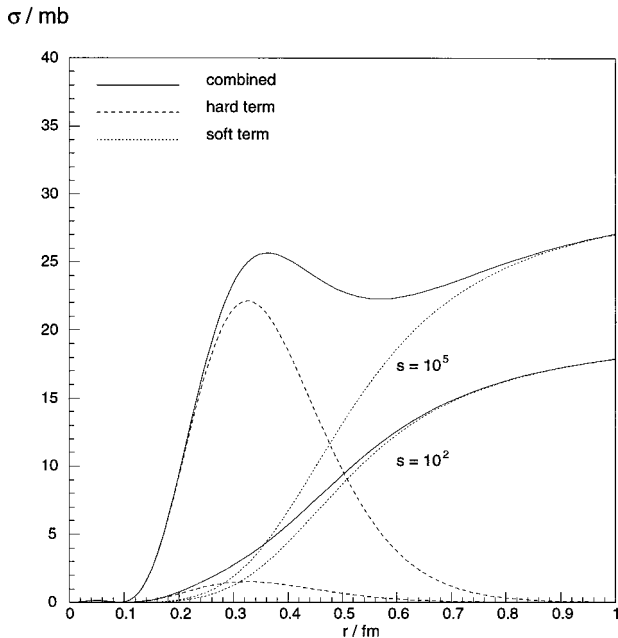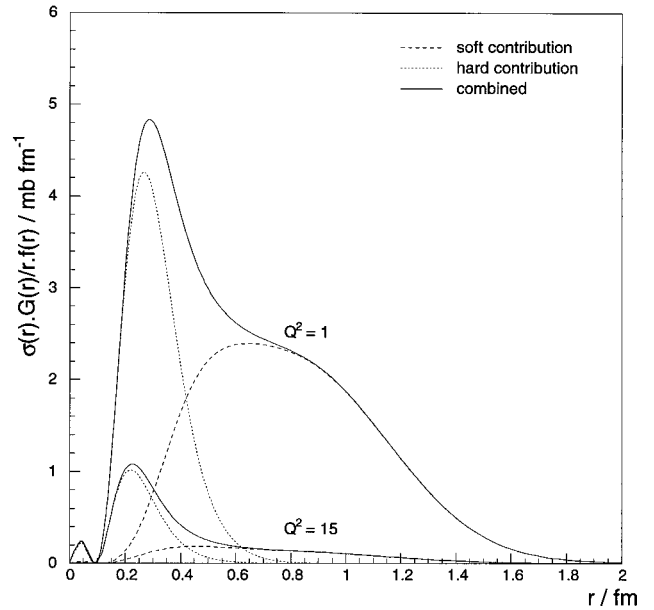
This form enables the width and height of the enhancement to be controlled independently while keeping a factor of close to unity at small r.

The resulting behavior of $G(r)$ is shown in Fig. 2 for the parameter values of our final fit I, described below. The behavior at both small and large r values is very similar to that suggested by a successful ''off-diagonal'' generalized vector dominance model [29], where the probability distribution of scattering eigenstates exhibits peaks for cross sections of
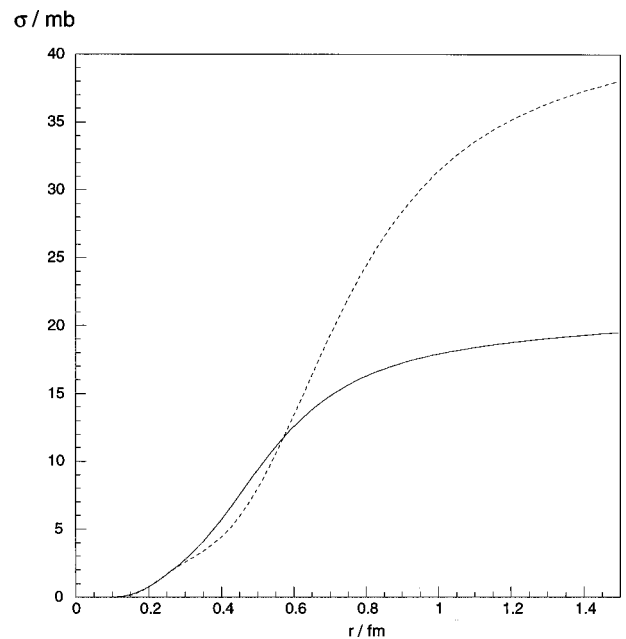

FIG. 6. Hard and soft contributions to the dipole cross section (fit I).

FIG. 8. Comparison of the dipole cross section of fit I (solid line) with that obtained in fit II (dotted line) at $s = 100$ GeV^2. The two fits were constrained to the ZEUS and H1 values for the diffractive ratio respectively.

TABLE III. Fit III, incorporating the charm contribution, with two mass squared parameters: m_L^2 for the light quarks and m_C^2 for the charm quark. The diffractive ratio is the same as for fit I.

Total χ^2 315 (0.89 per d.o.f.)			
λ_S	0.06 (fixed)	λ_H	0.380 ± 0.005
a_0^S	29.90 (fixed)		
a_1^S	0.056 ± 0.008	a_1^H	0.47 ± 0.05
a_2^S	-0.144 ± 0.004	a_2^H	2.5 ± 0.1
		a_3^H	-6.56 ± 0.07
		ν_H^2	4.22 ± 0.02
B	6.8 ± 0.1	c^2	0.342 ± 0.008
R	5.67 ± 0.03		
m_L^2	0.08 (fixed)	m_C^2	1.4 (fixed)

Photoabsorption data ($Q^2 = 0$)		
Data set	Number of points	χ^2 per data point
Caldwell	18	1.5
H1	1	2.2
ZEUS	1	4.0

hadronic size on an otherwise monotonic decrease with σ [30].

3. Fits with the modified wave function

On refitting the data, we were able to adjust the ratio of diffractive to total cross section for photoproduction to any reasonable value by adjusting the value of the saturation parameter a_0^S. In addition, we fixed the value of the exponent λ_S to ensure reasonable agreement with the high energy real photoabsorption data points, which are of low statistical significance, as described below. Two fits I and II are reported here and summarized in Tables I and II. They differ in that they give diffractive ratios at $\sqrt{s}$ of 180 GeV of 14% and 23% to agree to within 2% with ZEUS and H1 photoproduction values respectively. Since the fits are similar, we shall concentrate on fit I, commenting briefly on the comparison with fit II where appropriate.

The quality of the fit is illustrated in Fig. 3. The fit has a good χ^2 but not so low as to indicate overfitting and the contribution from the very precise intermediate photoabsorption data is reasonably small. At high energies, the photoabsorption total cross section lies somewhat above the ZEUS point especially, even though the soft term s exponent λ_S was given a slightly low value 0.06 compared to the canonical Donnachie-Landshoff [22] value of 0.08 to improve the agreement. However, these data values are low in comparison with a generalized vector dominance based extrapolation from low Q^2 ZEUS data [31]. As regards the hard term, its s exponent λ_H is consistent with the "hard Pomeron" intercept of 1.418 obtained by Donnachie and Landshoff [9].

The predictions for the ratio of diffractive to total cross section are shown in Fig. 4. As can be seen, there is little variation with Q^2, which accords with the Q^2 independence of $F_2^{D(2)}(\beta, Q^2)$. The weak s dependence is also in line with experiment [32].
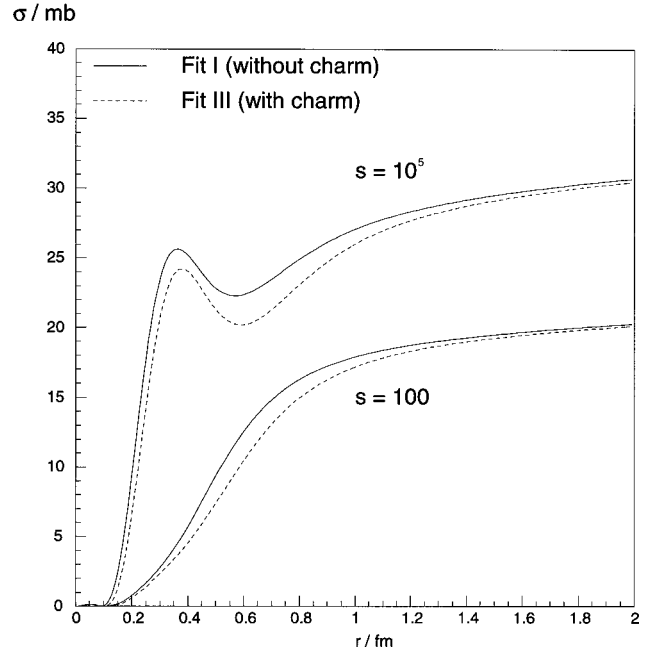

FIG. 9. Comparison at large and small energies of the dipole cross section of fit I with that obtained in fit III where a charm contribution was included.

4. Dipole cross section

The energy dependence of the dipole cross section resulting from fit I and its decomposition into hard and soft components are shown in Fig. 5 and Fig. 6 respectively. In addition, the contribution to the total photoabsorption cross section arising from dipoles of different sizes is shown in Fig. 7, showing that the dipole cross section is essentially unconstrained by the data for dipole sizes above about 1.5 fm. Below this the results accord well with reasonable physical expectations, with the soft Pomeron dominating the large r/low Q^2 behavior and the hard Pomeron dominating at low r/high Q^2 when the energy is high enough. In addition, dipoles of order 1 fm have cross sections commensurate with typical hadronic cross sections. The precise value is sensitive to the diffractive ratio imposed in photoproduction, as shown in Fig. 8, where the dipole cross sections resulting from fit I (with the ZEUS value imposed) and fit II (with the H1 value imposed) are compared.

5. Effect of charm

We have investigated the effect of including a charm contribution, assuming dipoles of the same transverse size have the same cross section irrespective of flavor. We have adopted a minimalist approach in assuming that the effect of charm flavor on the photon wave function occurs only through the charm mass, leaving the large r peak, $f(r)$, for example, unchanged. This leads to an additional term for $G(r)$, of the same form as before but with m_f^2 appropriate to a charmed quark, and weighted 2/3 in accordance with the
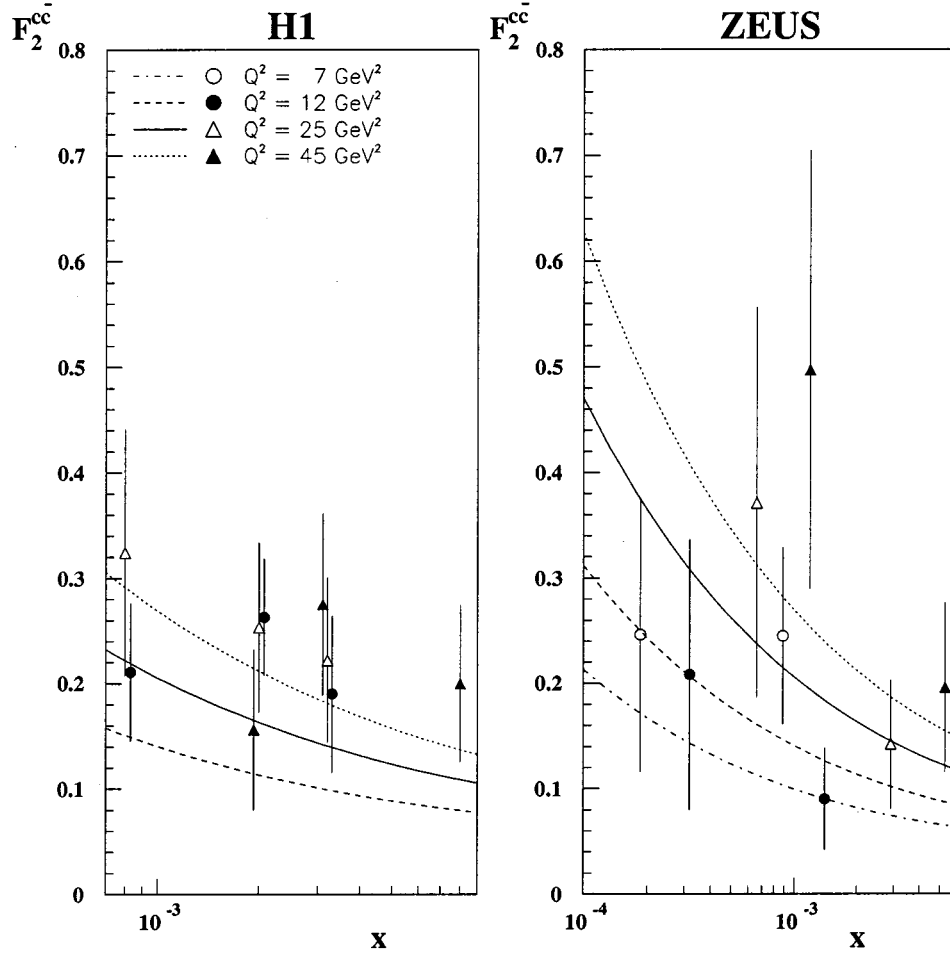
FIG. 10. Comparison of the charm structure function $F_2^{c\bar{c}}$ predicted from fit III ($m_C^2 = 1.4$ GeV^2) with experimental data [41,42]. (Points at the same x have been displaced slightly for clarity.)

squared charge coefficient of Eq. (14). The extra term has the effect of increasing the small dipole flux at large Q^2.

Details of a fit (fit III) which includes a contribution from charm with an assumed m_C^2 of 1.4 GeV^2 are given in Table III.[2] We have kept the same normalization parameter a_0^S as fit I to ensure the same diffractive ratio. A comparison of the resulting dipole cross section with that of fit I is displayed in Fig. 9.

As might be expected, the hard term of the dipole cross section is suppressed, while the soft term is little affected. Very little effect on the diffractive ratio is observed. A comparison of the predicted $F_2^{c\bar{c}}$ with data is given in Fig. 10 showing broad agreement. To gauge the effect of increasing the charm mass, we compare predictions from a fit (fit IV) having a larger m_C^2 of 2.3 GeV^2 with the same data in Fig.

———————

[2]The charm contribution will be significant for Q^2 values in the perturbative region, which makes a choice of a running quark mass appropriate. The charm mass is estimated by the Particle Data Group to lie in the range 1.1–1.4 GeV. [33]

11. Within the limitations of the data, the lower charm mass value is preferred.

6. Other approaches

A number of other authors have attempted to determine the dipole proton cross section [34,7,35,36,1,37,38]. The closest in spirit to our approach is that of Golec-Biernat and Wüsthoff [39], who achieve a good fit with a remarkably simple parametrization of the dipole cross section, which depends on r and x rather than r and s as here. Their approach also differs from our own in two other ways. First, they do not fit the accurate photoproduction data, so that they are less sensitive to large dipoles and consequently to confinement effects, and second, they impose saturation at low x (or high s) as well as at large interquark separations. Our own success in achieving a fit with no saturation in the energy variable indicates that the present data do not require it.

V. CONCLUSIONS

We have succeeded in obtaining a fit to photoabsorption data with $Q^2 \leq 60$ GeV^2, including real photon data, using a
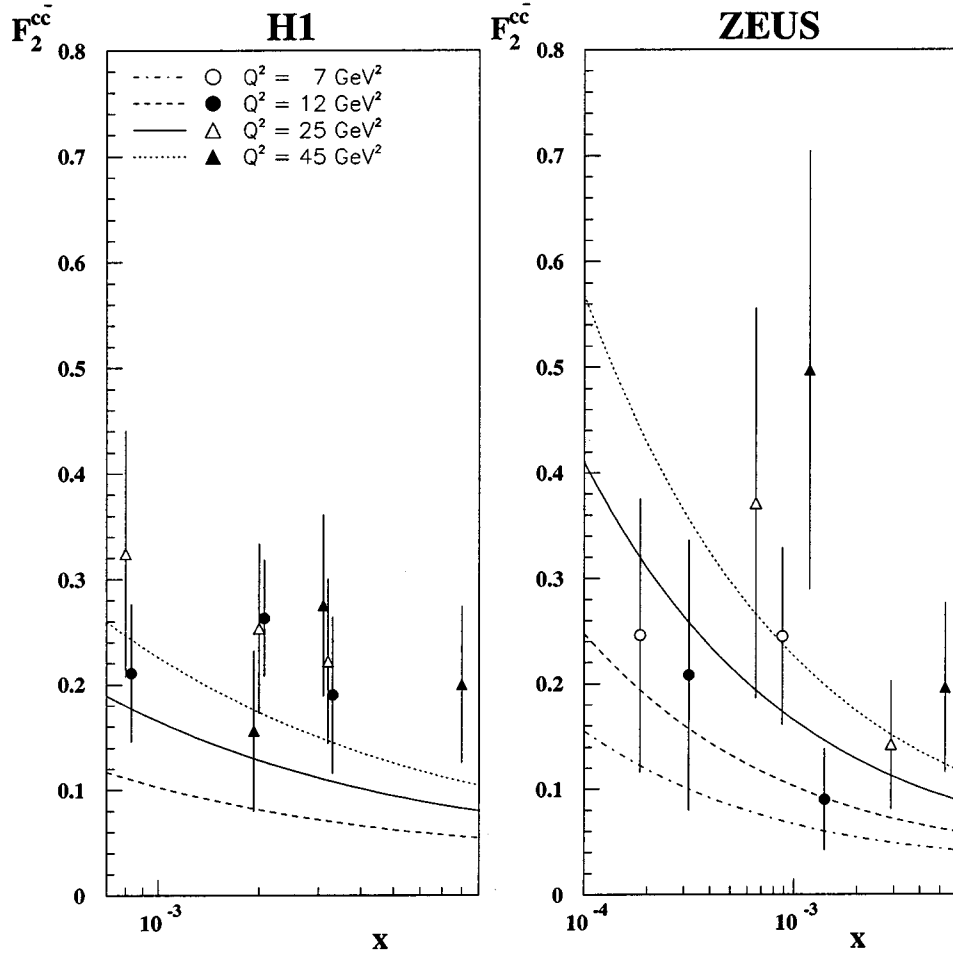
FIG. 11. Comparison of the charm structure function $F_2^{c\bar{c}}$ predicted from fit IV ($m_C^2 = 2.3\,\text{GeV}^2$) with experimental data [41,42]. (Points at the same x have been displaced slightly for clarity.)

parametrized form of the color dipole cross section. This has required modifying the effective photon wave function to take account of non-perturbative effects. The result is consistent with the cited experimental constraints from diffractive dissociation data.

The next step is to develop the model so as to address the more detailed diffractive dissociation experimental data in the form of the $F_2^{D(3)}$ structure function. Also, we should include contributions from higher Fock states, such as the $|q\bar{q}g\rangle$, which will dominate at low β [40].

We should also be able to apply our parametrization to the prediction of both vector meson production and deeply virtual Compton scattering cross sections.

[1] N. N. Nikolaev and B. G. Zakharov, Z. Phys. C **49**, 607 (1991).

[2] N. N. Nikolaev and B. G. Zakharov, Z. Phys. C **53**, 331 (1992).

[3] A. H. Mueller, Nucl. Phys. **B415**, 373 (1994).

[4] A. H. Mueller and B. Patel, Nucl. Phys. **B425**, 471 (1994).

[5] J. R. Forshaw, talk given at the Photon 97 conference, Egmond aan Zee, 1997, hep-ph/9707238.

[6] J. R. Forshaw and D. A. Ross, *Quantum Chromodynamics and the Pomeron* (Cambridge, England, 1997), Chap. 7.

[7] H. G. Dosch, T. Gousset, G. Kulzinger, and H. J. Pirner, Phys. Rev. D **55**, 2602 (1997).

[8] P. Moseley and G. Shaw, Phys. Rev. D **52**, 4941 (1995); G. Kerley and G. Shaw, *ibid.* **56**, 7291 (1997).

[9] A. Donnachie and P. V. Landshoff, Phys. Lett. B **437**, 408 (1998).

[10] A. Rostovtsev, M. G. Ryskin, and R. Engel, Phys. Rev. D **59**, 014021 (1999).

[11] N. N. Nikolaev and B. G. Zakharov, in *Nuclear Physics: At the Frontiers of Knowledge: Proceedings*, edited by Z.-X. Sun and J.-C. Xu (World Scientific, Singapore, 1996), p. 275.

[12] H1 Collaboration, S. Aid *et al.*, Nucl. Phys. **B470**, 3 (1996).

[13] H1 Collaboration, C. Adloff *et al.*, Nucl. Phys. **B497**, 3 (1997).

[14] ZEUS Collaboration, M. Derrick *et al.*, Z. Phys. C **72**, 399 (1996).

[15] ZEUS Collaboration, M. Derrick *et al.*, Z. Phys. C **69**, 607 (1996).

[16] ZEUS Collaboration, J. Breitweg *et al.*, Phys. Lett. B **407**, 432 (1997).

[17] ZEUS Collaboration, J. Breitweg *et al.*, Eur. Phys. J. C **7**, 609 (1999).

[18] E665 Collaboration, M. R. Adams *et al.*, Phys. Rev. D **54**, 3006 (1996).

[19] D. O. Caldwell *et al.*, Phys. Rev. Lett. **40**, 1222 (1978).

[20] S. Aid *et al.*, Z. Phys. C **69**, 27 (1995).

[21] ZEUS Collaboration, M. Derrick *et al.*, Z. Phys. C **63**, 391 (1994).

[22] A. Donnachie and P. V. Landshoff, Z. Phys. C **61**, 139 (1994).

[23] I. J. D. Craig and J. C. Brown, *Inverse Problems in Astronomy* (Hilger, Bristol, UK, 1986).

[24] T. J. Loredo and R. I. Epstein, Astrophys. J. **336**, 896 (1989).

[25] G. Grammar and J. D. Sullivan, in *Electromagnetic Interac-tions of Hadrons*, edited by A. Donnachie and G. Shaw (Plenum, New York, 1978), Vol. II, Chap. 4.

[26] ZEUS Collaboration, J. Breitweg *et al.*, Eur. Phys. J. C **1**, 81 (1998).

[27] H1 Collaboration, C. Adloff *et al.*, Z. Phys. C **74**, 221 (1997).

[28] ZEUS Collaboration, J. Breitweg *et al.*, Z. Phys. C **75**, 421 (1997).

[29] H. Fraas, B. J. Read, and D. Schildknecht, Nucl. Phys. **B86**, 346 (1975); G. Shaw, Phys. Rev. D **47**, R3676 (1993); A. Pautz and G. Shaw, Phys. Rev. C **57**, 2648 (1998), references therein.

[30] L. Frankfurt, V. Guzey, and M. Strikman, Phys. Rev. D **58**, 094039 (1998).

[31] A. Bornheim, talk given at the LISHEP conference, Rio de Janeiro, 1998.

[32] A. T. Doyle, talk given at the DIS98 conference, Brussels, 1998.

[33] Particle Data Group, C. Caso *et al.*, Eur. Phys. J. C **3**, 1 (1998).

[34] U. D'Alesio, A. Metz, and H. J. Pirner, hep-ph/9811349.

[35] H. G. Dosch, T. Gousset, and H. J. Pirner, Phys. Rev. D **57**, 1666 (1998).

[36] H. G. Dosch and M. Rüter, Phys. Rev. D **57**, 4097 (1998).

[37] J. Nemchik, N. N. Nikolaev, and E. Predazzi, Phys. Lett. B **374**, 199 (1996).

[38] J. Nemchik, N. N. Nikolaev, E. Predazzi and B. G. Zakaharov, Z. Phys. C **75**, 71 (1997).

[39] K. Golec-Biernat and M. Wüsthoff, Phys. Rev. D **59**, 014017 (1999).

[40] M. Wüsthoff, Phys. Rev. D **56**, 4311 (1997).

[41] C. Adloff *et al.*, Z. Phys. C **72**, 593 (1996).

[42] J. Breitweg *et al.*, Phys. Lett. B **407**, 402 (1997).